

## Differential Scattering of Metastable He( $2^3S$ ) on He( $1^1S$ ) at Energies between 5 and 10 eV\*

R. Morgenstern,<sup>†</sup> D. C. Lorents, J. R. Peterson, and R. E. Olson

Stanford Research Institute, Menlo Park, California 94025

(Received 10 May 1973)

Differential cross sections of the scattering of He( $2^3S$ ) on He( $1^1S$ ) at seven energies between 5 and 10 eV have been measured in a new apparatus. The cross sections display several types of structure. A large rainbow peak is observed at a reduced angle  $\tau = E\theta$  of approximately 161 eV deg for all energies. Fine structure on the rainbow peak and at smaller angles is also resolved. From the rainbow scattering we can deduce that the depth of the He<sub>2</sub>( $a^3\Sigma_u^+$ ) potential curve is  $D_e = 2.00$  eV. This value translates to a well depth for the  $A^1\Sigma_u^+$  state [He( $2^1S$ ) + He( $1^1S$ )] of 2.50 eV, which is in agreement with the latest spectroscopic analysis. At reduced scattering angles less than 120 eV deg the observed structure is not reproduced in the two-state elastic-scattering theoretical calculations based on the adiabatic states  $a^3\Sigma_u^+$  and  $c^3\Sigma_g^+$ . It is suggested that this disagreement is due to a strong interaction between the  $c^3\Sigma_g^+$  state of He( $2^3S$ ) + He( $1^1S$ ) and the  $b^3\Pi_g$  state of He( $2^3P$ ) + He( $1^1S$ ). This interaction severely modifies the differential elastic-scattering cross sections at angles less than 120 eV deg.

### I. INTRODUCTION

Recently, there has been an expanding interest in the interaction of rare-gas atoms in electronically excited states. Special interest has been directed to the He + He system in its various excited states,<sup>1-5</sup> because it is simple enough to allow accurate theoretical calculations and because there is good spectroscopic data available on it. Scattering studies can provide a valuable alternate method of studying these interactions.

In this paper we present differential cross sections in the 5–10 eV range (c.m. energy) for the scattering of He( $2^3S$ ) from He( $1^1S$ ). The measurements have two purposes: first, they provide a direct test of the adiabatic potential curves, which until now have only been known from spectroscopic data and theoretical calculations, and second, they provide information about the interactions between potential curves that lead to velocity-dependent nonadiabatic transitions.

Previous scattering experiments on this system<sup>3</sup> were made at thermal energies and could only sample the interactions at large separations of the collision partners. Our experiments were conducted at collision energies high enough to surmount the long-range potential barriers and yield information about the potential wells.

Owing to the symmetry of the He<sub>2</sub> wave functions, the potentials consist of gerade and ungerade curves for both the He( $2^3S$ ) + He( $1^1S$ ) and the He( $2^1S$ ) + He( $1^1S$ ) collision systems. As summarized by Ginter and Battino,<sup>1</sup> both the He<sub>2</sub>( $a^3\Sigma_u^+$ ) and the He<sub>2</sub>( $A^1\Sigma_u^+$ ) molecular states are members of a Rydberg series, converging to He<sub>2</sub><sup>+</sup>( $X^2\Sigma_u^+$ ).

The energy spacings between the minima of all these potential curves have been accurately determined spectroscopically. Therefore, if one knows the well depth relative to the separated atom limit of one of these curves, one can deduce the depths of the others.

The He<sub>2</sub>( $A^1\Sigma_u^+$ ) curve is known from the analysis of emission and absorption spectra arising from transitions between this state and the ground-state He<sub>2</sub>( $X^1\Sigma_g^+$ ).<sup>4</sup> The He<sub>2</sub><sup>+</sup>( $X^2\Sigma_u^+$ ) curve is known from scattering experiments<sup>6-8</sup> and also from *ab initio* calculations.<sup>9</sup> The data concerning the He<sub>2</sub>( $a^3\Sigma_u^+$ ) curve obtained from the measurements presented here, can thus be compared with various experimental and theoretical parameters that exist for the other curves. These potentials, in schematic form, are shown in Fig. 1.

We can also expect to obtain information about the  $c^3\Sigma_g^+$  state, since half of the collisions proceed through this state. The scattering pattern for this state is expected to show rainbow features due both to a minimum and a maximum in the potential curve. For this state the potential minimum is quite well determined from spectroscopic data, but the hump region is poorly known.

### II. APPARATUS

Figure 2 shows the experimental setup. It consists of two separately pumped chambers that are connected by an aperture for the beam, 3.5 mm in diam. The base pressure in the system is  $3 \times 10^{-7}$  torr. The pressure in the ion-source chamber rises to  $1 \times 10^{-5}$  torr when the source is on, and the pressure in the main chamber rises to  $7 \times 10^{-7}$  torr when the target gas is admitted.

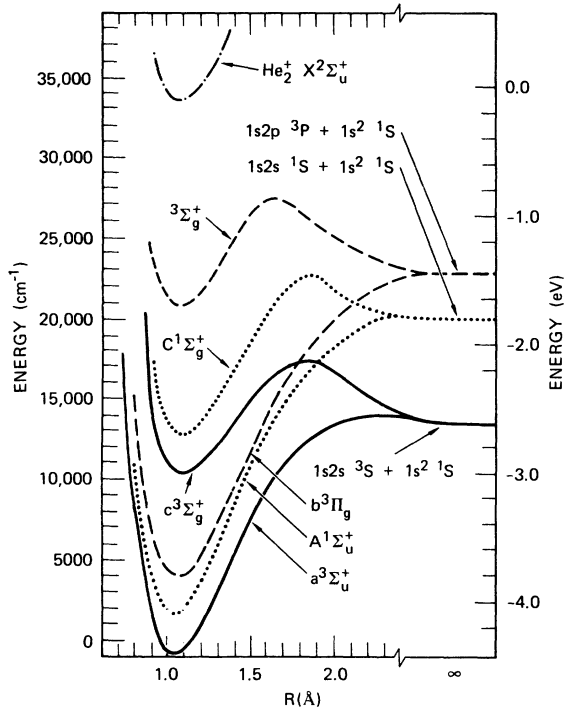


FIG. 1. Relevant  $\text{He}_2$  potential curves. These curves were taken from Ref. 1, and do not show the more accurate potentials, derived from Refs. 4 and 6–9, and confirmed in this work.

#### A. Beam

The metastable He beam is obtained by near-resonant charge exchange of a  $\text{He}^+$  ion beam (10–20 eV) with alkali-metal atoms.  $\text{He}^+$  ions are produced in a discharge source. After a first focusing in an einzel lens, the beam is shifted

parallel to itself by two pairs of deflector plates to prevent fast neutrals produced near the source from entering the scattering cell. The beam is then focused by a second einzel lens and enters the charge-exchange oven, which contains the Cs vapor. Ions that are not neutralized are swept out of the beam behind the oven, and, after passing another aperture, the beam enters the scattering cell. A Faraday cage can be moved into the beam to measure the ion-beam intensity entering the gas cell.

The distance from the ion source to the oven is 31 cm and from the oven to the scattering cell 20.5 cm. The beam is collimated by the oven-entrance aperture (1.5 mm diam) and the aperture in front of the Faraday cage (1 mm diam). The beam intensity is stable within  $\sim 10\%$  over several days after an initial unstable period of  $\sim 1$  day. This long-term stability is achieved by regulating the discharge current in the ion source, using a feedback loop that controls the filament.

#### B. Gas Target

The target gas is confined in a small semicylindrical gas cell, which has an entrance aperture of 1.6 mm (larger than the beam diameter) to ensure that the beam does not hit the metal. The exit slit is rectangular with a vertical height of 1.7 mm and a length that allows observation of particles scattered horizontally between  $-25^\circ$  and  $+70^\circ$  from the beam axis. The length of the target volume (distance from entrance and exit apertures) is 12.5 mm. The He pressure in the cell was  $3 \times 10^{-4}$  torr, as measured with a MKS Baratron. To obtain background corrections on

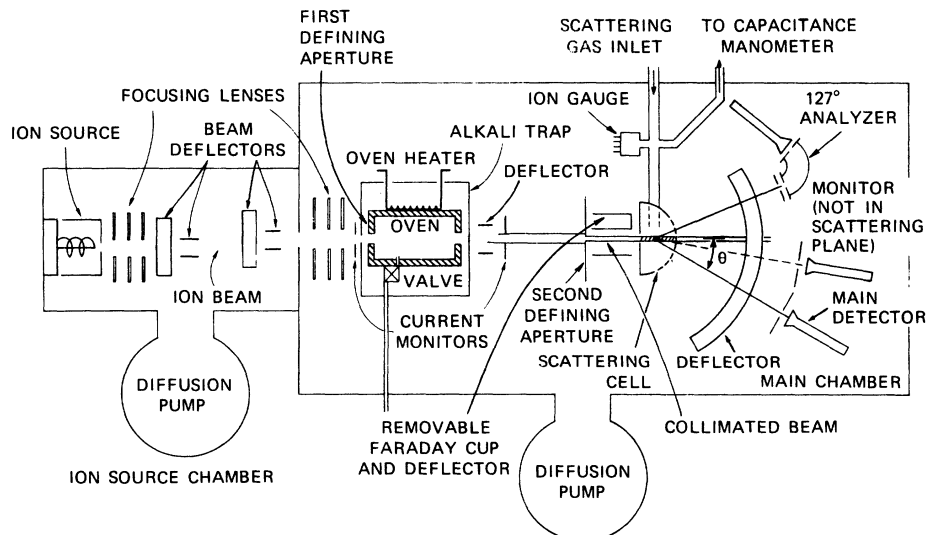


FIG. 2. Schematic diagram of apparatus.

the scattering signal, gas at the same flow rate can be admitted directly to the main chamber instead of into the target cell.

### C. Detection System

The apparatus contains three detectors, all equipped with channel-electron multipliers (CEM).

The main scattered neutral detector essentially consists of a CEM behind an aperture 1.6 mm wide by 4.4 mm high; the distance from scattering center to CEM is 28.1 cm. Ions can be deflected from the detector by deflector plates between the scattering center and detector. It can be rotated in a horizontal plane around the scattering center and sees the whole intersection of beam and target gas at every angle. Therefore, the signal is directly proportional to the differential cross section and no angular correction is necessary. The angular resolution changes with angle and is  $\sim 0.4^\circ$ ,  $0.5^\circ$ ,  $0.8^\circ$ , and  $1.5^\circ$  for  $\theta = 5^\circ$ ,  $10^\circ$ ,  $20^\circ$ , and  $60^\circ$ , respectively. To correct for scattering by the residual gas in the main chamber we always measured alternately the signals with the target gas first admitted to the cell and then admitted directly into the main chamber at the same flow rate. The difference in these two signals is due only to scattering in the gas cell.

Another detector consists of a combination of retarding field and  $127^\circ$  energy analyzer, followed by a CEM. It is also rotatable and is used in this experiment for an accurate determination of the ion energy.

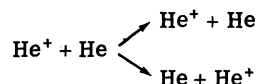
The monitor detector is a CEM located in the vertical plane through the beam axis at a fixed angle of  $\sim 10^\circ$ . It observes charged, as well as neutral, particles coming from the scattering center, and serves to monitor the scattered intensity.

The main detector signals are stored in a multi-channel analyzer, which accumulates the scattering signal in a single channel at each angle until the monitor detector has accumulated a certain predetermined number of pulses. This is a normalization that compensates for fluctuations in beam intensity and target gas pressure. The main detector is then automatically shifted to the next angle, and its output is accumulated in the next channel of the multiscaler. Thus, the data for each angle are obtained automatically, and long integration times can be used to enhance signal-to-noise ratios. All measurements were reproduced at corresponding angles on both sides of the beam to ensure symmetry about the beam axis.

Since a considerable amount of ground-state He atoms may be present in our beam and may pro-

duce part of the scattering signal, the relative detection efficiencies of our detectors for metastables and ground-state atoms is important.

The efficiency of metastables to produce secondary electrons on metal surfaces is known to be in the range 0.5 to 1, even at thermal energies.<sup>10</sup> The efficiency of ground-state atoms is known to decrease sharply at low energies<sup>11</sup> but the actual behavior depends largely on the surface conditions. To obtain the relative efficiencies for our CEM detectors we measured the differential cross sections for the two processes



Owing to the symmetry of these two processes, the cross sections oscillate with the same amplitude, but at  $180^\circ$  out of phase.<sup>12</sup> The ratio of the measured amplitude of these oscillations for He and  $\text{He}^+$ , which was derived from the scattering signal with and without deflection of the  $\text{He}^+$ , gives directly the ratio of detection efficiencies. This efficiency ratio is shown in Fig. 3. Assuming the  $\text{He}^+$  efficiency to be lower than 0.5 at 20 eV,<sup>11</sup> the He efficiency turns out to be lower than  $10^{-3}$ . This ensures that our scattering signal did not contain an appreciable contribution due to scattering of ground-state He atoms.

### D. Metastable-Beam Characteristics

There are two important characteristics of the neutral beam that must be determined in order to correctly analyze and interpret the data: (i) the kinetic energy of the metastables and (ii) the

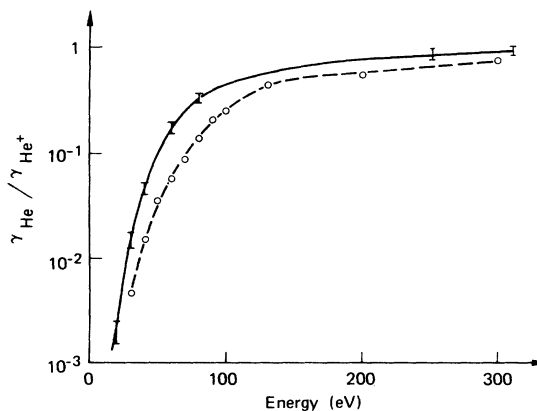


FIG. 3. Detector efficiency for ground-state He relative to  $\text{He}^+$ . Solid curve: channeltron detector with the funnel biased 20 V negative, this work; dashed curve: secondary-emission measurements of Hayden and Utterback (Ref. 11).

relative population of the two metastable He states ( $2^1S$  and  $2^3S$ ) in the beam. The determination of these properties is not trivial, and considerable effort was given to it.

The energy of the neutrals deviates considerably from the ion energy for two reasons. First, the ion energy inside the charge-exchange oven is different from that outside, owing to the contact potential between the alkali-metal layer and the stainless-steel walls. Second, the charge-exchange process itself leads to a small energy shift, depending on how close in energy the initial and final electronic states match.

We determine the kinetic energy of the metastables by the following method: The ion energy is measured with a  $127^\circ$  analyzer and the energy difference between ions and neutrals is determined by a time-of-flight measurement. The beam is pulsed by sweeping it across the entrance aperture of the charge-exchange oven at a rate of  $\sim 100$  kHz. Particles with different energies arrive at the detector at different times and the distribution of arrival times is measured by time-to-pulse height conversion in combination with pulse-height analysis in a multichannel analyzer. The time resolution is  $\sim 0.3 \mu\text{sec}$  and mainly due to the velocity distribution in the beam. The energy of the metastables is found to be lower than the ion energy by  $\Delta E = 2 \pm 0.2$  eV for the case of Cs vapor in the oven at all energies used in this experiment.

Charge transfer of  $\text{He}^+$  ions in alkali-metal vapors is known to be an efficient method of producing fast excited He beams.<sup>13</sup> He atoms produced in the near-resonant reactions are expected<sup>14</sup> to be in some combination of the  $2^1S$ ,  $2^1P$ ,  $2^3S$ , and  $2^1P$  states. Radiative decay of the  $P$  states rapidly produces a new combination of ground state  $1^1S$ , and the metastables  $2^1S$  and  $2^3S$ . Because of the long metastable lifetimes (20 m/sec<sup>15</sup> and 8000 sec,<sup>16</sup> respectively), these relative populations remain unchanged during the short flight times ( $< 2 \times 10^{-5}$  sec) between the charge-transfer oven and the collision volume in this experiment. Since our detector system can discriminate against the ground-state atoms, but is incapable of distinguishing between the  $2^1S$  and  $2^3S$  atoms, it is clearly desirable to have a single-component metastable population. There are several observations, which, when taken together, strongly indicate that the charge-exchange process  $\text{He}^+ + \text{Cs} \rightarrow \text{He}^* + \text{Cs}^+$  at energies below  $\sim 30$  eV produces  $\text{He}(2^3S)$  metastables nearly exclusively and only negligible amounts of  $\text{He}(2^1S)$ . Olson and Smith<sup>17</sup> have recently concluded from theoretical arguments that although the closest energy match for the system  $\text{He}^+ + \text{Cs}$  and  $\text{He}^* + \text{Cs}^+$  is to the

$\text{He}(2^1S)$  state (+0.078 eV energy defect), the charge exchange goes mainly to the  $\text{He}(2^3P)$  and  $\text{He}(2^1P)$  states (energy defect  $-0.271$  and  $-0.525$  eV, respectively). Since the  $\text{He}(2^1P)$  decays rapidly to the ground state and the  $\text{He}(2^3P)$  decays to  $\text{He}(2^3S)$ , the only metastables that reach the scattering center are  $\text{He}(2^3S)$ .

These theoretical arguments are supported by the time-of-flight measurements of the energy distribution of the metastables. Figure 4 shows the time-of-flight spectrum for ions and metastables at 20 eV. The peak width is mainly due to the initial energy distribution of the ion, as checked by a combined measurement with the  $127^\circ$  analyzer and time-of-flight analysis. The energy spread of the neutral particles appears to be only slightly larger than that of the ions (0.73 vs 0.66 eV). This indicates that of the two initial states  $\text{He}(2^1S)$  or  $\text{He}(2^3P)$  (energy difference 0.35 eV), one is produced in an amount at least seven times larger than the other. On the basis of Olson and Smith's calculation, we conclude that  $\text{He}(2^3P)$  is the larger component.

Another indication that mainly  $\text{He}(2^3S)$  is present in the beam comes from measurements by Lepri, *et al.*<sup>18</sup> who examined the energies of Penning electrons from the process  $\text{He}^* + \text{Ar}$ ,  $\text{Xe}$ . The  $\text{He}^*$  in their experiments was produced by charge exchange with K and Cs, and at energies below  $\sim 30$  eV they observed contributions to the electron spectra arising from  $\text{He}(2^3S)$  but not from  $\text{He}(2^1S)$  metastables.

Finally, the scattering results presented in Sec. III show by the lack of rainbow structure due to the  $A^1\Sigma_u^+$  state that we had a pure  $\text{He}(2^3S)$  beam.

All the measurements reported here are made with Cs charge-exchange vapor. However, it may be of interest to note that measurements with  $\text{He}^*$  beams obtained from charge exchange with K produced the same scattering patterns as those obtained using Cs vapor. Apparently, both charge-

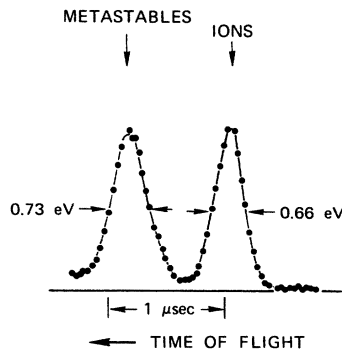


FIG. 4. Time-of-flight spectrum of ions and metastables.

exchange processes yield mainly  $\text{He}(2^3\text{S})$  metastables at these energies.

### III. RESULTS AND DISCUSSION

The experimentally determined differential cross sections are shown in Fig. 5. The measured scattering signal  $\sigma$  is reduced to  $\rho = \sigma \theta \sin \theta$  and plotted versus  $\tau = E \theta$  ( $E = \text{collision energy}$ ,  $\theta = \text{scattering angle}$ , both in the center of mass units). This reduction serves to display features in the cross section at the same  $\tau$  value which are due to scattering at the same impact parameter, even if they are obtained at different collision energies.<sup>19</sup> Absolute cross sections were not obtained because no satisfactory method of measuring the intensity of metastables in the beam was available.

From our knowledge of the  $\text{He}_2(a^3\Sigma_u^+)$  and the  $\text{He}_2(c^3\Sigma_g^+)$  potential curves one can expect the following structures in the cross sections: A rainbow peak at  $\tau \approx 160$  eV deg, due to scattering from the deep minimum ( $\sim 2$  eV) of the  $a^3\Sigma_u^+$  curve; a second rainbow at  $\tau \approx 75$  eV deg, due to the well of the  $c^3\Sigma_g^+$  curve, and a third one at  $\tau \approx 65$  eV deg, due to the outside hump of the  $c^3\Sigma_g^+$  curve. If  $\text{He}(2^1\text{S})$  metastables were also present in the beam, another rainbow at  $\tau \approx 200$  eV deg would appear, due to the deep well ( $\approx 2.5$  eV) of the  $A^1\Sigma_u^+$

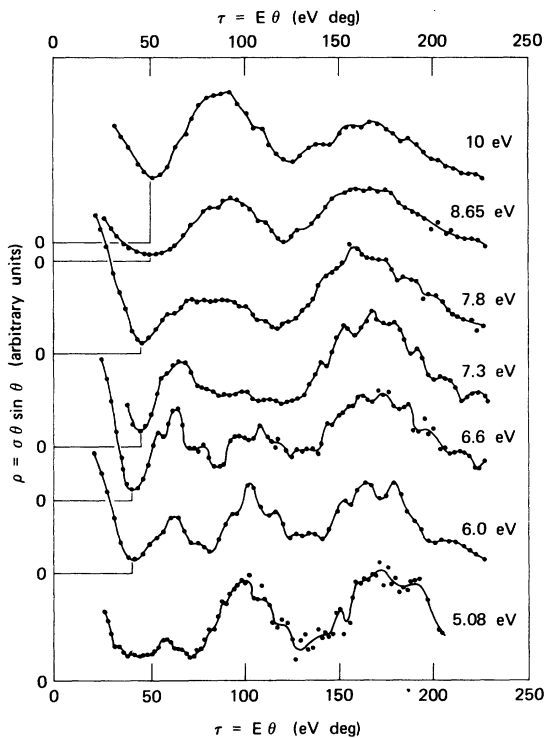


FIG. 5. Measured differential cross sections for scattering of  $\text{He}(2^3\text{S})$  by  $\text{He}(1^1\text{S})$ .

curve. While there is a lot of structure between  $\tau = 40$  and  $\tau = 190$ , we observed no rainbow structure at  $\tau \approx 200$ . This is a strong indication that our experiments were performed with a nearly pure  $\text{He}(2^3\text{S})$  metastable beam, as discussed above. Ground-state atoms cannot contribute to the observed structure because, in addition to their low detection efficiency of less than  $10^{-3}$ , the  $\text{He}_2(X^1\Sigma_g^+)$  potential curve is practically monotonically repulsive<sup>20</sup> and can only lead to a smooth contribution in the scattering cross section. Therefore, it appears to be justified to interpret all the observed structure as due to  $\text{He}(2^3\text{S}) + \text{He}$  collisions.

For all collision energies there appears a pronounced rainbow structure peaked at  $\tau \approx 164$  eV deg. In Fig. 6 the two-state differential elastic-

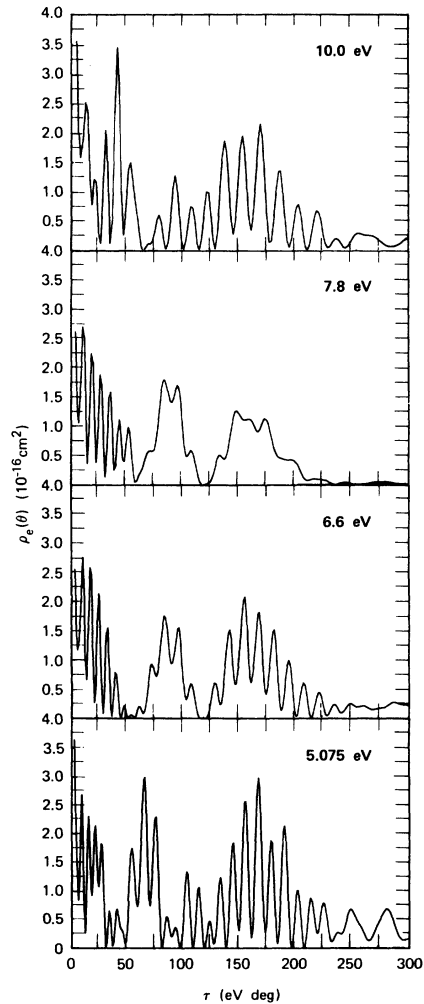


FIG. 6. Two-state elastic-scattering cross sections calculated from the potentials of Ginter and Battino. The well depth of the  $a^3\Sigma_u^+$  state has been lowered to 2.00 eV.

scattering cross sections calculated from the spectroscopic  $a$ - and  $c$ -state potentials show this rainbow structure. Superimposed on the calculated differential cross sections is a fine structure with a frequency of approximately  $\Delta\tau \approx 15$  eV deg. This structure is associated with the rainbow scattering and is due to an interference caused by scattering at the same angle from positive and negative values of the deflection function. At large- $\tau$  values  $\approx 250$  eV deg, regular oscillations with a frequency of approximately  $\Delta\tau \approx 30$  eV deg are present. These are nuclear-symmetry oscillations caused by the indistinguishability of the projectile and target particles.

The calculations are based on spline fits to the potential curves given by Ginter and Battino,<sup>1</sup> where the  $u$  and  $g$  potential curves in the region of the minima were shifted together to obtain various well depths. The humps at large separations were held at the values shown by Ginter and Battino. At large internuclear distances,  $R > 2.3$  Å, the  $u$  potential curve was calculated using

$$V_u(R) = \alpha R^2 e^{-\beta R}. \quad (1)$$

$\beta$  was set equal to  $1.6a_0^{-1}$ , the same as Evans and Lane,<sup>5</sup> but  $\alpha$  was set equal to 0.1263 a.u., which was chosen to match the curves of Ginter and Battino at 2.3 Å. The  $g$ -state potential curve for these separations was set equal to

$$V_g(R) = V_u(R) + \lambda e^{-\gamma R}. \quad (2)$$

Here  $\lambda$  and  $\gamma$  were set equal to 1.54 a.u. and  $1.43a_0^{-1}$ , respectively; the same as used in Ref. 5. The  $u$  and  $g$  potential curves of Ginter and Battino were extended to small internuclear distance,  $R < 0.8$  Å, by fitting the  $u$  curve to a Morse potential in the bowl region. The  $g$  curve was extended to small separations by using the same parametrization as given by Eq. (2). Here,  $\lambda$  was set equal to 0.137 a.u., the united atom separation of the  $g$  and  $u$  curves.<sup>5</sup> The exponential factor  $\gamma$  was varied to join the spline-fit  $g$  potential at 0.8 Å. For the calculations presented here,  $\gamma = 0.471a_0^{-1}$  for values of  $R < 0.8$  Å.

Using the above potential forms the elastic two-state differential cross sections were calculated with WKB phase shifts using a partial-wave summation, with nuclear symmetry included. The cross sections obtained from this calculation are shown in Fig. 6. The formulas are well known and need not be presented here.<sup>6</sup> The best agreement between theory and experiment with respect to the rainbow position at  $\tau \approx 164$  eV deg occurred when the  $u$ -state well depth was set equal to 2.00 eV. Owing to an uncertainty in the kinetic energies of the metastables of  $\sim 0.25$  eV, this derived value

of the well depth is uncertain by  $\sim 0.04$  eV. An additional uncertainty is produced by the fact that the maximum of the rainbow structure cannot easily be determined in the theoretical or experimental curves, owing to the overlying fine structure. While there is reasonable agreement between theory and experiment at large- $\tau$  values, the energy-dependent structure observed on the cross sections for angles  $\tau \lesssim 140$  eV deg is not reproduced in the calculations.

At energies between 5 and 6.6 eV, two peaks at  $\tau \approx 60$  and  $\tau \approx 100$ , which might be the two expected rainbow structures of the  $c^3\Sigma_g^+$  scattering, are observed in the data. At higher energies, however, these peaks appear to merge into one broad peak with its maximum at  $\tau \approx 90$  eV deg. In contrast the two-state calculation exhibits only one main peak in this region.

The potential curves for the He<sub>2</sub>( $a^3\Sigma_u^+$ ) and He<sub>2</sub>( $c^3\Sigma_g^+$ ) states are well enough known to conclude that the reasons for this disagreement cannot be incorrect values of the well depth, the position of the well, or an improper shape of the involved potential curves. Therefore, other reasons must be considered

Interactions with other potential curves, leading to inelastic processes may be the reason for the disagreement between measured and calculated cross sections. Since we do not analyze the energy of the scattered particles, our scattering signal may be due to both elastically and inelastically scattered particles.

Analysis of the He\*+He potentials shown in Fig. 1 indicates that there are two possible inelastic channels open for loss of elastic flux. One possible channel is the  $^3\Sigma_g^+$  state that dissociates to He(1s2p,  $^3P$ )+He. This curve lies close to the  $c^3\Sigma_g^+$  potential curve over a considerable range of internuclear separations. The two states are connected by radial coupling. This possible inelastic process has been studied previously by Evans, Cohen, and Lane,<sup>21</sup> who found the cross sections for excitation into the  $^3\Sigma_g^+$ He(2<sup>3</sup>P)+He(1<sup>1</sup>S) channel to be very small at low energies ( $Q = 5.0 \times 10^{-20}$  cm<sup>2</sup> at 5 eV rising to only  $2.2 \times 10^{-19}$  cm<sup>2</sup> at 10 eV).

Another possible inelastic channel is the  $b^3\Pi_g$  potential curve that dissociates to He(1s2p,  $^3P_1$ )+He(1<sup>1</sup>S) and crosses the  $c^3\Sigma_g^+$  potential curve at approximately  $R = 3.2a_0$ . These two curves lie within 0.1 eV for internuclear separations of  $2.35a_0 < R < 3.75a_0$  and are connected by rotational coupling.

Lenamon, Browne, and Olson<sup>22</sup> have calculated the inelastic cross section for this exit channel to help understand the measurements presented here. They find the transition probabilities into

the  $b^3\Pi_g$  state are almost unity, and the resulting inelastic total cross sections are very large. At 8.65 eV the total inelastic cross section is  $1.42 \times 10^{-16} \text{ cm}^2$ . The calculated inelastic differential cross section exhibits a peak in the region of  $\tau = 85 \text{ eV deg}$ .

Obviously this strong interaction will perturb the scattering in the  $\text{He}_2(c^3\Sigma_g^+)$  potential curve. An extreme assumption would be that the contribution from the  $\text{He}_2(c^3\Sigma_g^+)$  curve to the structure of the scattering cross section is completely removed owing to inelastic losses and to a complete disturbance of the scattering phases. In that case all of the measured structures for  $40 < \tau < 140 \text{ eV deg}$  correspond to scattering from the  $a^3\Sigma_u^+$  state and are supernumeraries belonging to the main rainbow at  $\tau = 164 \text{ eV deg}$ . Figure 7 shows calculated cross sections which are only due to the  $\text{He}_2(a^3\Sigma_u^+)$  curve. This assumption seems too

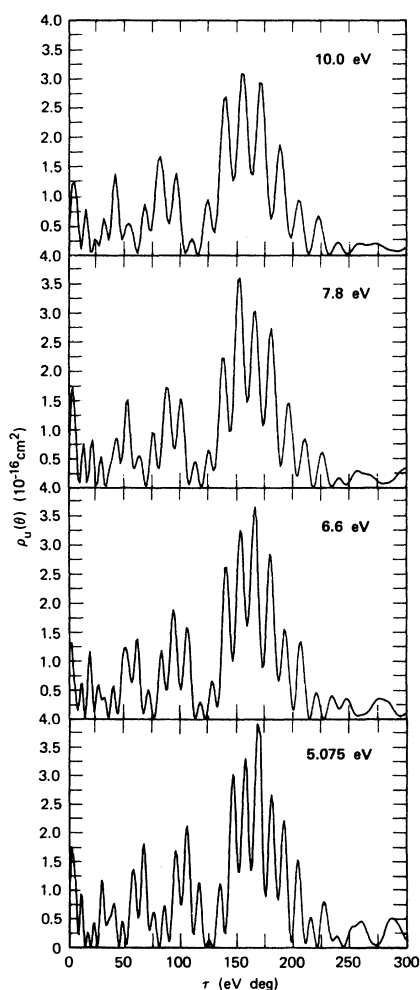


FIG. 7. Theoretical cross sections, ungerade state only.

extreme, since it yields cross sections that agree with experiment at energies between 5 and 6.6 eV but definitely disagree at higher energies.

Three-state calculations made at 5, 10, and 25 eV indicate the effect that the rotational coupling to the  $b^3\Pi_g$  state will have on the elastic scattering (Fig. 6 of Ref. 22). The elastic cross sections are calculated with (three state) and without (two state) the inelastic channel. The cross sections are found to change drastically at  $\tau \lesssim 120 \text{ eV deg}$  when the inelastic channel is included. Most noticeably, a strong peak is found to appear around  $\tau = 85 \text{ eV deg}$ , and the structure in the range  $50 < \tau < 120 \text{ eV deg}$ , as well as the main rainbow peak, is found to be altered. Such effects have been termed elastic perturbations<sup>23,24</sup> and for the case where there are large inelastic transition probabilities, as in this system, the effects on the elastic scattering can be quite large. Moreover, the position of the elastic perturbation peak at  $\tau \approx 85 \text{ eV deg}$  can be expected to be relatively invariant with energy.

Therefore, the disagreement between theory and experiment is considerably reduced when the interaction with the  $b^3\Pi_g$  state is included. The large peak growing at the higher energies at  $\tau \approx 90 \text{ eV deg}$  is attributed to the elastic perturbation and also to an underlying inelastic peak that occurs near this  $\tau$  value<sup>22</sup> and is included in the experimental signal. The observed decrease in the magnitude of the main rainbow peak at  $\sim 160 \text{ eV deg}$  at higher energies is also predicted by the three-state calculations.

The fast oscillations are definitely observed throughout the measured scattering, although they are not well resolved. They were observed in repeated measurements at the same energy, and although the positions of the peaks are strongly energy dependent, the basic frequency is reproducible. These oscillations can be very important in determining an accurate description of the scattering potentials. In our case, however, the observed frequency is in fair agreement with the calculated value, and we believe that the potentials used in the calculations are as accurate as the experimental data can ascertain. Since the coarse structure for  $\tau < 120 \text{ eV deg}$ , which apparently is due to at least three states, is difficult to understand, we have not attempted to draw any further conclusions from the fine structure.

#### IV. CONCLUSIONS

Differential scattering cross sections for the collision system  $\text{He}(2^3S) + \text{He}(1^1S)$  have been measured in the energy range from 5 to 10 eV. The well depth of the  $\text{He}_2(a^3\Sigma_u^+)$  potential curve

is determined from the position of the main rainbow structure to be  $D_e = 2.00 \pm 0.05$  eV. Using optical data, as described in Ref. 1, one can obtain the well depths of the  $\text{He}_2(A^1\Sigma_u^+)$  and the  $\text{He}_2^+(X^2\Sigma_u^+)$  curves. Doing this, we get a value of  $D_e = 2.50 \pm 0.05$  eV for both of these well depths. This is in agreement with the value obtained from the analysis of emission and absorption spectra in He.<sup>4</sup> It is also in agreement with the calculations of Liu<sup>9</sup> for the dissociation energy of  $\text{He}_2^+$ .

Our measured scattering cross sections cannot be completely explained by pure two-state scat-

tering. It is concluded that a strong rotational interaction between the  $c^3\Sigma_g^+$  and  $b^3\Pi_g$  states gives rise to a perturbation of the elastic scattering as well as to an inelastic transition to  $\text{He}(2^3P)$ . The inelastic transition has recently been observed by energy analysis of the scattered particles using a time-of-flight method.<sup>25</sup>

#### ACKNOWLEDGMENTS

R. Morgenstern gratefully acknowledges a grant from the Deutsche Forschungsgemeinschaft.

\*Work supported by the National Science Foundation under Grant Nos. GP-21314A and GA-33418.

† Present address: Physikalisches Institut Universität, 78 Freiburg, Germany.

<sup>1</sup>M. L. Ginter and R. Battino, *J. Chem. Phys.* **52**, 4469 (1970).

<sup>2</sup>M. L. Ginter and C. M. Brown, *J. Chem. Phys.* **56**, 672 (1972).

<sup>3</sup>H. Haberland, C. H. Chen, and Y. T. Lee, *Atomic Physics 3*, edited by S. J. Smith and G. K. Walters (Plenum, New York, 1973), p. 339.

<sup>4</sup>K. M. Sando, *Mol. Phys.* **23**, 413 (1972).

<sup>5</sup>S. A. Evans and N. F. Lane, *Phys. Rev.* **188**, 268 (1969).

<sup>6</sup>R. E. Olson and C. R. Mueller, *J. Chem. Phys.* **46**, 3810 (1967).

<sup>7</sup>H. P. Weise, H. N. Mittmann, A. Ding, and A. Henglein, *Z. Naturforsch. A* **26**, 1122 (1971).

<sup>8</sup>W. G. Rich, Ph.D. thesis (College of William and Mary, 1972) (unpublished).

<sup>9</sup>B. Liu, *Phys. Rev. Lett.* **27**, 1251 (1971).

<sup>10</sup>F. B. Dunning, A. C. H. Smith, and R. F. Stebbings, *J. Phys. B* **4**, 1683 (1971).

<sup>11</sup>H. C. Hayden and N. G. Utterback, *Phys. Rev.* **135**, A1575 (1964).

<sup>12</sup>R. P. Marchi and F. T. Smith, *Phys. Rev.* **139**, A1025 (1965).

<sup>13</sup>M. Hollstein, J. R. Sheridan, J. R. Peterson, and D. C. Lorents, *Phys. Rev.* **187**, 118 (1969).

<sup>14</sup>J. R. Peterson and D. C. Lorents, *Phys. Rev.* **182**, 152 (1969).

<sup>15</sup>G. W. F. Drake, *Phys. Rev. A* **3**, 908 (1971).

<sup>16</sup>R. S. Van Dyck, C. E. Johnson, and H. A. Shugart, *Phys. Rev. A* **4**, 1327 (1971).

<sup>17</sup>R. E. Olson and F. T. Smith, *Phys. Rev. A* **7**, 1529 (1973).

<sup>18</sup>M. Lepri, R. Hammond, and J. W. Dubrin, *Chem. Phys. Lett.* **19**, 271 (1973).

<sup>19</sup>F. T. Smith, R. P. Marchi, and K. G. Dedrick, *Phys. Rev.* **150**, 79 (1966).

<sup>20</sup>R. G. Gordon and Y. S. Kim, *J. Chem. Phys.* **56**, 3122 (1972).

<sup>21</sup>S. A. Evans, Y. S. Cohen, and N. F. Lane, *Phys. Rev. A* **4**, 2235 (1971).

<sup>22</sup>L. Lenamon, J. C. Brown, and R. E. Olson, following paper *Phys. Rev.* **8**, 2380 (1973).

<sup>23</sup>F. T. Smith, D. C. Lorents, W. Aberth, and R. P. Marchi, *Phys. Rev. Lett.* **15**, 742 (1965).

<sup>24</sup>R. E. Olson and F. T. Smith, *Phys. Rev. A* **3**, 1607 (1971).

<sup>25</sup>R. E. Olson, R. Morgenstern, D. C. Lorents, J. C. Browne, and L. Lenamon, second following paper, *Phys. Rev.* **8**, 2387 (1973).